

# Direct Data Detection of OFDM Signals Over Wireless Channels

A. Saci, *Student Member, IEEE*, A. Al-Dweik, *Senior Member, IEEE*, A. Shami, *Senior Member, IEEE*

## Abstract

This paper presents a novel efficient receiver design for wireless communication systems that incorporate orthogonal frequency division multiplexing (OFDM) transmission. The proposed receiver does not require channel estimation or equalization to perform coherent data detection. Instead, channel estimation, equalization, and data detection are combined into a single operation, and hence, the detector is denoted as direct data detector ( $D^3$ ). The performance of the proposed system is thoroughly analyzed theoretically in terms of bit error rate (BER), and validated by Monte Carlo simulations. The obtained theoretical and simulation results demonstrate that the BER of the proposed  $D^3$  is only 3 dB away from coherent detectors with perfect knowledge of the channel state information (CSI) in flat fading channels, and similarly in frequency-selective channels for a wide range of signal-to-noise ratios (SNRs). If CSI is not known perfectly, then the  $D^3$  outperforms the coherent detector substantially, particularly at high SNRs with linear interpolation. The computational complexity of the  $D^3$  depends on the length of the sequence to be detected, nevertheless, a significant complexity reduction can be achieved using the Viterbi algorithm.

## Index Terms

OFDM, fading channels, data detection, Viterbi, sequence detection, channel estimation, equalization.

A. Saci, A. Al-Dweik and A. Shami are with the Department of Electrical and Computer Engineering, Western University, London, ON, Canada, (e-mail: {asaci, aaldweik, abdallah.shami}@uwo.ca).

A. Al-Dweik is also with the Department of Electrical and Computer Engineering, Khalifa University, Abu Dhabi, UAE, (e-mail: dweik@kustar.ac.ae).

Part of this work is protected by the US patent: A. Al-Dweik "Signal detection in a communication system." U.S. Patent No. 9,596,119. 14 Mar. 2017.

## I. INTRODUCTION

Orthogonal frequency division multiplexing (OFDM) is widely adopted in several wired and wireless communication standards, such as digital audio broadcasting (DAB) [1], digital video broadcasting terrestrial (DVB-T) [2], worldwide interoperability for microwave access (WiMAX) technologies [3], and the Long Term Evolution-Advanced (LTE-A) standard [4]. OFDM is also a strong candidate for the fifth generation of wireless networks (5G) [5].

One of the main advantages of OFDM is that each subcarrier experiences flat fading even though the overall signal spectrum suffers from frequency-selective fading. Moreover, incorporating the concept of cyclic prefix (CP) prevents inter-symbol-interference (ISI) if the CP length is larger than the maximum delay spread of the channel. Consequently, a low-complexity single-tap equalizer can be utilized to eliminate the impact of the multipath fading channel. Under such circumstances, the OFDM demodulation process can be performed once the fading parameters at each subcarrier, commonly denoted as channel state information (CSI), is known accurately. Therefore, robust channel estimation techniques should be invoked to avoid performance degradation [6]-[18].

In general, channel estimation can be classified into blind [6]-[11], and pilot-aided techniques [12]-[18]. Blind channel estimation techniques are spectrally efficient because they do not require any overhead to estimate the CSI, nevertheless, such techniques have not yet been adopted in practical OFDM systems. Conversely, pilot-based CSI estimation is preferred for practical systems, because typically it is more robust and less complex. In pilot-based CSI estimation, the pilot symbols are embedded within the subcarriers of the transmitted OFDM signal in time and frequency domain; hence, the pilots form a two dimensional (2-D) grid [2], [4]. The density of the pilot symbols depends on the frequency-selectivity and time variation of the channel, or equivalently, the coherence bandwidth and coherence time of the channel. The channel response at the pilot symbols can be obtained using least-square (LS) frequency domain estimation; and the channel parameters at other subcarriers can be obtained using various interpolation techniques [19]. The density of the pilot grid and the interpolation technique used creates a compromise among the error performance, spectral efficiency, and computational complexity. The spectral efficiency is determined by the pilots' density, which has to satisfy the 2-D sampling theorem. The computational complexity is determined by the interpolation technique, optimal interpolation requires a 2-D Wiener filter that exploits the time and frequency correlation of the channel,

however, it is substantially complex to implement [20]. In time-varying channels, the spectral efficiency can be enhanced by changing the pilots' grid structure adaptively based on the channel conditions [21]. The complexity can be reduced by decomposing the 2-D interpolation process into two cascaded 1-D processes, and then, using less computationally-involved interpolation schemes [22], [23]. Low complexity interpolation, however, is usually accompanied with error rate performance degradation [23]. It is also worth noting that most practical OFDM-based systems utilize a fixed grid pattern structure [2], [4]. Moreover, the standards allow changing the power of the pilot symbols based on the CSI. At low SNRs, the pilot symbols' power can be boosted by an additional 3 or 6 dB [4].

Once the channel parameters are obtained for all subcarriers, the received samples at the output of the fast Fourier transform (FFT) are equalized to compensate for the channel fading. Fortunately, the equalization for OFDM is performed in the frequency domain using single-tap equalizers. The equalizer output samples, which are denoted as the decision variables, will be applied to a maximum likelihood detector (MLD) to regenerate the information symbols.

Unlike conventional OFDM detection, this work presents a new approach to regenerate the information symbols directly from the received samples at the FFT output. Thus, there is no need to perform channel estimation, interpolation, equalization, or detection operations. The proposed system exploits the fact that the channel coefficients over adjacent subcarriers are highly correlated and approximately equal, and hence, such information is used to estimate the transmitted data sequence. Consequently, the proposed detector is denoted as direct data detector ( $D^3$ ).

The rest of this paper is organized as follows. The OFDM system and channel models are described in Section II. The proposed  $D^3$  is presented in Section III, and efficient implementation of the  $D^3$  is explored in Section IV. The system error probability performance analysis is presented in Section V. Complexity analysis of the conventional pilot based OFDM and the  $D^3$  are given in Section VI. Numerical results are discussed in Section VII, and finally, the conclusion is drawn in Section VIII.

In what follows, unless otherwise specified, uppercase boldface and blackboard letters such as  $\mathbf{H}$  and  $\mathbb{H}$ , will denote  $N \times N$  matrices, whereas lowercase boldface letters such as  $\mathbf{x}$  will denote row or column vectors with  $N$  elements. Uppercase, lowercase, or bold letters with a tilde such as  $\tilde{d}$  will denote trial values, and symbols with a hat, such as  $\hat{\mathbf{x}}$ , will denote the estimate of  $\mathbf{x}$ . Letters with apostrophe such as  $v'$  are used to denote the next value, i.e.,  $v' \triangleq v + 1$ . Furthermore,

$\mathbb{E}[\cdot]$  denotes the expectation operation.

## II. SIGNAL AND CHANNEL MODELS

Consider an OFDM system with  $N$  subcarriers modulated by a sequence of  $N$  complex data symbols  $\mathbf{d} = [d_0, d_1, \dots, d_{N-1}]^T$ . The data symbols are selected uniformly from a general constellation such as  $M$ -ary phase shift keying (MPSK), quadrature amplitude modulation (QAM) or  $M$ -ary amplitude shift keying (MASK). In conventional pilot-aided OFDM systems [24],  $N_P$  of the subcarriers are allocated for pilot symbols, which can be used for channel estimation/synchronization purposes. The modulation process in OFDM can be implemented efficiently using an  $N$ -point inverse FFT (IFFT) algorithm, where its output during the  $\ell$ th OFDM block can be written as,

$$\mathbf{x}(\ell) = \mathbf{F}^H \mathbf{d}(\ell) \quad (1)$$

where  $\mathbf{F}$  is the normalized  $N \times N$  FFT matrix, and hence,  $\mathbf{F}^H$  is the IFFT matrix. The elements of  $\mathbf{F}^H$  are defined as  $F_{i,v} = (1/\sqrt{N})e^{j2\pi iv/N}$  where  $i$  and  $v$  denote the row and column indices  $[i, v] \in \{0, 1, \dots, N-1\}$ , respectively. In order to simplify the notation, the block index  $\ell$  is dropped for the remaining parts of the paper unless it is necessary to include it. To combat ISI between consecutive OFDM symbols and maintain the subcarriers' orthogonality in frequency-selective multipath fading channels, a CP of length  $N_{CP}$  samples, no less than the channel maximum delay spread ( $\mathcal{D}_h$ ), is formed by copying the last  $N_{CP}$  samples of  $\mathbf{x}$  and appending them in front of the IFFT output to compose the OFDM symbol with a total length  $N_t = N + N_{CP}$  samples and a duration of  $T_t$  seconds. Then, the complex baseband OFDM symbol during the  $\ell$ th signaling period  $\hat{\mathbf{x}}$  is upsampled, filtered and up-converted to a radio frequency centered at  $f_c$  before transmission through the antenna.

At the receiver front-end, the received signal is down-converted to baseband and sampled at a rate  $T_s = T_t/N_t$ . In this work, the channel is assumed to be composed of  $\mathcal{D}_h + 1$  independent multipath components each of which has a gain  $h_m \sim \mathcal{CN}(0, 2\sigma_{h_m}^2)$  and delay  $m \times T_s$ , where  $m \in \{0, 1, \dots, \mathcal{D}_h\}$ . A quasi-static channel is assumed throughout this work, and thus, the channel taps are considered constant over one OFDM symbol, but they may change over two consecutive symbols. Therefore, the received sequence consists of  $N_t$  samples, and can be expressed as,

$$\hat{\mathbf{y}} = \mathbb{H}\hat{\mathbf{x}} + \hat{\mathbf{z}} \quad (2)$$

where the channel matrix  $\hat{\mathbb{H}}$  is an  $N_t \times N_t$  Toeplitz matrix with  $h_0$  on the principal diagonal and  $h_1, \dots, h_{\mathcal{D}_h}$  on the minor diagonals, respectively, the elements of the noise vector  $\hat{\mathbf{z}}$  are modeled as a complex additive white Gaussian noise (AWGN) random variables with zero mean and variance  $2\sigma_z^2 = \mathbb{E}[|z_n|^2]$ . The received non CP samples that belong to a single OFDM symbol can be expressed as,

$$y_n = \sum_{m=0}^{\mathcal{D}_h} h_m x_{\langle n-m \rangle_N} + z_n \quad (3)$$

where  $\langle \cdot \rangle_N$  denotes the modulo  $N$  operation. Subsequently, the receiver discards the first  $N_{\text{CP}}$  samples, and computes the FFT of  $\mathbf{y}$ , where  $\mathbf{y} = \mathbb{H}\mathbf{x} + \mathbf{z}$ , the channel matrix  $\mathbb{H}$  is an  $N \times N$  circulant matrix. Therefore, the FFT output can be computed as

$$\begin{aligned} \mathbf{r} &= \mathbf{F} \mathbf{y} \\ &= \mathbf{F} \mathbb{H} \mathbf{F}^H \mathbf{d} + \mathbf{F} \mathbf{z}. \end{aligned} \quad (4)$$

Because the matrix  $\mathbb{H}$  is circulant, it will be diagonalized by the FFT and IFFT matrices. Thus,

$$\mathbf{r} = \mathbf{H} \mathbf{d} + \mathbf{w} \quad (5)$$

where  $\{\mathbf{r}, \mathbf{w}\} \in \mathbb{C}^{N \times 1}$ ,  $w_v \sim \mathcal{CN}(0, 2\sigma_w^2)$  is the FFT of the noise vector  $\mathbf{z}$ , and  $\mathbf{H}$  denotes the channel frequency response (CFR)

$$\mathbf{H} = \text{diag} \{[H_0, H_1, \dots, H_{N-1}]\}. \quad (6)$$

By noting that  $\mathbf{r}|_{\mathbf{H}, \mathbf{d}} \sim \mathcal{CN}(\mathbf{H}\mathbf{d}, 2\sigma_w^2 \mathbf{I}_N)$  where  $\mathbf{I}_N$  is an  $N \times N$  identity matrix, then it is straightforward to show that the MLD can be expressed as

$$\hat{\mathbf{d}} = \arg \min_{\tilde{\mathbf{d}}} \left\| \mathbf{r} - \mathbf{H} \tilde{\mathbf{d}} \right\|^2 \quad (7)$$

where  $\|\cdot\|$  denotes the Euclidean norm, and  $\tilde{\mathbf{d}} = [\tilde{d}_0, \tilde{d}_1, \dots, \tilde{d}_{N-1}]^T$  denotes the trial values of  $\mathbf{d}$ . As can be noted from (7), the MLD requires the knowledge of  $\mathbf{H}$ . Moreover, because (7) describes the detection of more than one symbol, it is typically denoted as maximum likelihood sequence detector (MLSD). If the elements of  $\mathbf{d}$  are independent, the MLSD can be replaced by a symbol-by-symbol MLD

$$\hat{d}_v = \arg \min_{\tilde{d}_v} \left| r_v - H_v \tilde{d}_v \right|^2. \quad (8)$$

Since perfect knowledge of  $\mathbf{H}$  is infeasible, an estimated version of  $\mathbf{H}$ , denoted as  $\hat{\mathbf{H}}$ , can be used in (7) and (8) instead of  $\mathbf{H}$ . Another possible approach to implement the detector is to

equalize  $\mathbf{r}$ , and then use a symbol-by-symbol MLD. Given that zero-forcing equalizer is used, then the equalized received sequence can be expressed as,

$$\check{\mathbf{r}} = \left[ \hat{\mathbf{H}}^H \hat{\mathbf{H}} \right]^{-1} \hat{\mathbf{H}}^H \mathbf{r} \quad (9)$$

and

$$\hat{d}_v = \arg \min_{\tilde{d}_v} \left| \check{r}_v - \tilde{d}_v \right|^2, \forall v. \quad (10)$$

It is interesting to note that solving (7) does not necessarily require the explicit knowledge of  $\mathbf{H}$  under some special circumstances. For example, Wu and Kam [25] noticed that in flat fading channels, i.e.,  $H_v = H \forall v$ , it is possible to detect the data symbols using the following multiple-symbol differential detector (MSDD),

$$\hat{\mathbf{d}} = \arg \max_{\tilde{\mathbf{d}}} \frac{\left| \tilde{\mathbf{d}}^H \mathbf{r} \right|^2}{\left\| \tilde{\mathbf{d}} \right\|^2}. \quad (11)$$

Although the detector described in (11) is efficient in the sense that it does not require the knowledge of  $\mathbf{H}$ , its bit error rate (BER) performance is very sensitive to the channel variations.

### III. PROPOSED $D^3$ SYSTEM MODEL

One of the distinctive features of OFDM is that its channel coefficients over adjacent subcarriers in the frequency domain are highly correlated and approximately equal. The correlation coefficient between two adjacent subcarriers can be defined as

$$\begin{aligned} \rho_f &\triangleq \mathbb{E} [H_v H_v^*] \\ &= \mathbb{E} \left[ \sum_{n=0}^{\mathcal{D}_h} h_n e^{-j2\pi \frac{nv}{N}} \sum_{m=0}^{\mathcal{D}_h} h_m^* e^{j2\pi \frac{mv}{N}} \right] \\ &= \sum_{m=0}^{\mathcal{D}_h} \sigma_{h_m}^2 e^{j2\pi \frac{mv}{N}} \end{aligned} \quad (12)$$

where  $\sigma_{h_m}^2 = \mathbb{E} [|h_m|^2]$ . The difference between two adjacent channel coefficients is

$$\begin{aligned} \Delta_f &= \mathbb{E} [H_v - H_v] \\ &= \mathbb{E} \left[ \sum_{m=0}^{\mathcal{D}_h} h_m e^{-j2\pi \frac{mv}{N}} (1 - e^{-j2\pi \frac{m}{N}}) \right] \end{aligned} \quad (13)$$

For large values of  $N$ , it is straightforward to show that  $\varrho_f \rightarrow 1$  and  $\Delta_f \rightarrow 0$ . Similar to the frequency domain, the time domain correlation defined according to the Jakes' model can be computed as [26],

$$\begin{aligned}\varrho_t &= \text{E} \left[ H_v^\ell \left( H_v^{\hat{\ell}} \right)^* \right] \\ &= J_0 \left( 2\pi f_d T_s \right)\end{aligned}\quad (14)$$

where  $J_0(\cdot)$  is the Bessel function of the first kind and 0 order,  $f_d$  is the maximum Doppler frequency. For large values of  $N$ ,  $2\pi f_d T_s \ll 1$ , and hence  $J_0(2\pi f_d T_s) \approx 1$ , and thus  $\varrho_t \approx 1$ . Using the same argument, the difference in the time domain  $\Delta_t \triangleq \text{E} \left[ H_v^\ell - H_v^{\hat{\ell}} \right] \approx 0$ . Although the proposed system can be applied in the time domain, frequency domain, or both, the focus of this work is the frequency domain.

Based on the aforementioned properties of OFDM, a simple approach to extract the information symbols from the received sequence  $\mathbf{r}$  can be designed by minimizing the difference of the channel coefficients between adjacent subcarriers, which can be expressed as

$$\hat{\mathbf{d}} = \arg \min_{\tilde{\mathbf{d}}} \sum_{v=0}^{N-2} \left| \frac{r_v}{\tilde{d}_v} - \frac{r_{v+1}}{\tilde{d}_{v+1}} \right|^2. \quad (15)$$

As can be noted from (15), the estimated data sequence  $\hat{\mathbf{d}}$  can be obtained without the knowledge of  $\mathbf{H}$ . Moreover, there are no constraints on the channel coefficients, and hence, the  $D^3$  should perform fairly well even in frequency-selective fading channels. Nevertheless, it can be noted that (15) does not have a unique solution because  $\mathbf{d}$  and  $-\mathbf{d}$  can actually minimize (15). To resolve the phase ambiguity problem, one or more pilot symbols can be used as a part of the sequence  $\mathbf{d}$ . In such scenarios, the performance of the  $D^3$  will be affected indirectly by the frequency selectivity of the channel because the capability of the pilot to resolve the phase ambiguity depends on its fading coefficient. Another advantage of using pilot symbols is that it will not be necessary to detect the  $N$  symbols simultaneously. Instead, it will be sufficient to detect  $\mathcal{K}$  symbols at a time, which can be exploited to simplify the system design and analysis.

Using the same approach of the frequency domain, the  $D^3$  can be designed to work in the time domain as well by minimizing the channel coefficients over two consecutive subcarriers, i.e., two subcarriers with the same index over two consecutive OFDM symbols, which is also applicable to single carrier systems. It can be also designed to work in both time and frequency domains, where the detector can be described as

$$\hat{\mathbf{D}}_{\mathcal{L},\mathcal{K}} = \arg \min_{\tilde{\mathbf{D}}_{\mathcal{L},\mathcal{K}}} J \left( \tilde{\mathbf{D}}_{\mathcal{L},\mathcal{K}} \right) \quad (16)$$

where  $\mathbf{D}_{\mathcal{L},\mathcal{K}}$  is an  $\mathcal{L} \times \mathcal{K}$  data matrix,  $\mathcal{L}$  and  $\mathcal{K}$  are the time and frequency detection window size, and the objective function  $J(\tilde{\mathbf{D}})$  is given by

$$J(\tilde{\mathbf{D}}_{\mathcal{L},\mathcal{K}}) = \sum_{\ell=0}^{\mathcal{L}-1} \sum_{v=0}^{\mathcal{K}-2} \left| \frac{r_v^\ell}{\tilde{d}_v^\ell} - \frac{r_{\hat{v}}^\ell}{\tilde{d}_{\hat{v}}^\ell} \right|^2 + \left| \frac{r_v^\ell}{\tilde{d}_v^\ell} - \frac{r_v^{\ell'}}{\tilde{d}_v^{\ell'}} \right|^2. \quad (17)$$

For example, if the detection window size is chosen to be the LTE resource block, then,  $\mathcal{L} = 14$  and  $\mathcal{K} = 12$ . Moreover, the system presented in (17) can be extended to the multi-branch receiver scenarios, single-input multiple-output (SIMO) as,

$$\hat{\mathbf{D}} = \arg \min_{\tilde{\mathbf{d}}} \sum_{n=1}^{\mathcal{N}} \sum_{\ell=0}^{\mathcal{L}-1} \sum_{v=0}^{\mathcal{K}-2} \left| \frac{r_v^{\ell,n}}{\tilde{d}_v^\ell} - \frac{r_{\hat{v}}^{\ell,n}}{\tilde{d}_{\hat{v}}^\ell} \right|^2 + \left| \frac{r_v^{\ell,n}}{\tilde{d}_v^\ell} - \frac{r_v^{\ell',n}}{\tilde{d}_v^{\ell'}} \right|^2 \quad (18)$$

where  $\mathcal{N}$  is the number of receiving antennas.

#### IV. EFFICIENT IMPLEMENTATION OF $D^3$

It can be noted from (16) and (17) that solving for  $\hat{\mathbf{D}}$ , given that  $N_P$  pilot symbols are used, requires an  $M^{\mathcal{K} \times \mathcal{L} - N_P}$  trials if brute force search is adopted, which is prohibitively complex, and thus, reducing the computational complexity is crucial. Towards this goal, the two dimensional (2-D) resource block can be divided into a number of one-dimensional (1-D) segments in time and frequency domains. The main requirement is that each 1-D segment should contain at least one pilot symbol. Fig. 1 shows an example of a possible segmentation of a 2-D resource block into several 1-D segments over time and frequency.

Furthermore, by noting that the expression in (15) corresponds to the sum of correlated terms, which can be modeled as a first-order Markov process, then MLSD techniques such as the Viterbi algorithm can be used to implement the  $D^3$  efficiently. For example, the trellis diagram of the Viterbi algorithm with binary phase shift keying (BPSK) is shown in Fig. 2, and can be implemented as follows:

- 1) Initialize the path metrics  $\{\Gamma_0^U, \hat{\Gamma}_0^U, \Gamma_0^L, \hat{\Gamma}_0^L\} = 0$ , where  $U$  and  $L$  denote the upper and lower branches, respectively. Since BPSK is used, the number of states is 2.
- 2) Initialize the counter,  $c = 0$ .
- 3) Compute the branch metric  $J_{m,n}^c = \left| \frac{r_c}{m} - \frac{r_c}{n} \right|^2$ , where  $m$  is current symbol index,  $m = 0 \rightarrow \tilde{d} = -1$ , and  $m = 1 \rightarrow \tilde{d} = 1$ , and  $n$  is the next symbol index using the same mapping as  $m$ .



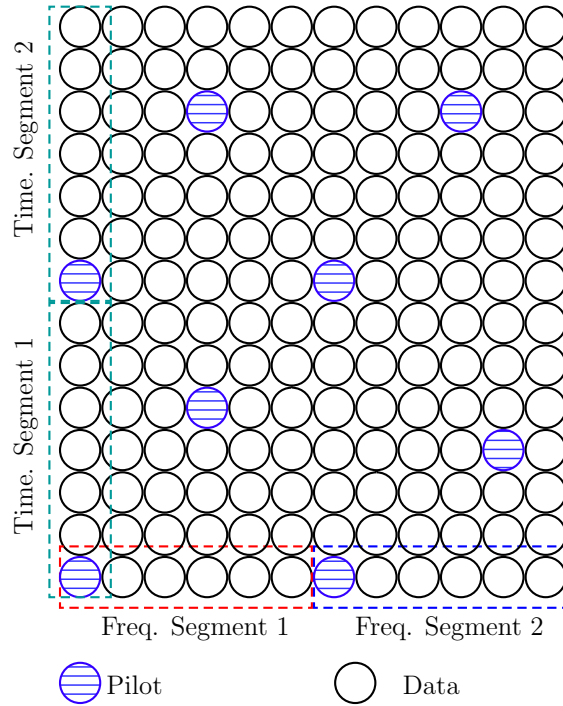


Fig. 1. Example of a 1-D segmentation over the frequency domain.

- 4) Compute the path metrics using the following rules,

$$\Gamma_{\dot{c}}^U = \min \left[ \Gamma_c^U, \dot{\Gamma}_c^U \right] + J_{00}^c$$

$$\dot{\Gamma}_{\dot{c}}^U = \min \left[ \Gamma_c^U, \dot{\Gamma}_c^U \right] + J_{10}^c$$

$$\Gamma_{\dot{c}}^L = \min \left[ \Gamma_c^L, \dot{\Gamma}_c^L \right] + J_{01}^c$$

$$\dot{\Gamma}_{\dot{c}}^L = \min \left[ \Gamma_c^L, \dot{\Gamma}_c^L \right] + J_{11}^c$$

- 5) Track the surviving paths, 2 paths in the case of BPSK.  
 6) Increase the counter,  $c := c + 1$ .  
 7) if  $c = \mathcal{K}$ , the algorithm ends. Otherwise, go to step 3.

It is worth mentioning that placing a pilot symbol at the edge of a segment terminates the trellis. To simplify the discussion, assume that the pilot value is  $-1$ , and thus we compute only  $J_{0,0}$  and  $J_{1,0}$ . Consequently, long data sequences can be divided into smaller segments bounded by pilots, which can reduce the delay by performing the detection over the sub-segments in parallel without sacrificing the error rate performance.

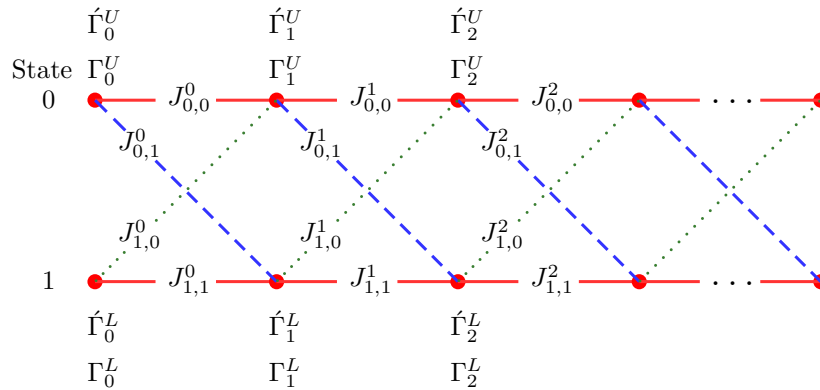


Fig. 2. Trellis diagram of the  $D^3$  detector for BPSK.

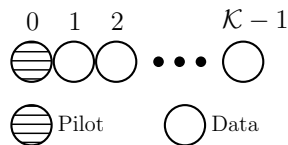


Fig. 3. Single-sided pilot segment.

### V. ERROR RATE ANALYSIS OF THE $D^3$

The system BER analysis is presented for several cases according to the pilot/data arrangements and pilot power boosting. For simplicity, each case is discussed in separate subsections. To make the analysis tractable, we consider BPSK modulation in the analysis while the BER of higher order modulations is obtained via Monte Carlo simulations.

#### A. Single-Sided Pilot

To detect a data segment that contains  $\mathcal{K}$  symbols, at least one pilot symbol should be part of the segment in order to resolve the phase ambiguity problem. Consequently, the analysis in this subsection considers the case where there is only one pilot within the  $\mathcal{K}$  symbols, as shown in Fig. 3. Given that the FFT output vector  $\mathbf{r} = [r_0, r_1, \dots, r_{N-1}]$  is divided into  $L$  segments each of which consists of  $\mathcal{K}$  symbols, including the pilot symbol, then the frequency domain  $D^3$  detector of the can be written as,

$$\hat{\mathbf{d}}_l = \arg \min_{\tilde{\mathbf{d}}} \sum_{v=l}^{\mathcal{K}-2+l} \left| \frac{r_v}{\tilde{d}_v} - \frac{r_{\hat{v}}}{\tilde{d}_{\hat{v}}} \right|^2 \quad \mathcal{K} \in \{2, 3, \dots, N-1\} \quad (19)$$

where  $l$  denotes the index of the first subcarrier in the segment, and without loss of generality, we consider that  $l = 0$ . Therefore, by expanding (19) we obtain,

$$\hat{\mathbf{d}}_0 = \arg \min_{\tilde{\mathbf{d}}} \left( \frac{r_0}{\tilde{d}_0} - \frac{r_1}{\tilde{d}_1} \right) \left( \frac{r_0}{\tilde{d}_0} - \frac{r_1}{\tilde{d}_1} \right)^* + \dots + \left( \frac{r_{\mathcal{K}-2}}{\tilde{d}_{\mathcal{K}-2}} - \frac{r_{\mathcal{K}-1}}{\tilde{d}_{\mathcal{K}-1}} \right) \left( \frac{r_{\mathcal{K}-2}}{\tilde{d}_{\mathcal{K}-2}} - \frac{r_{\mathcal{K}-1}}{\tilde{d}_{\mathcal{K}-1}} \right)^* \quad (20)$$

which can be simplified to,

$$\hat{\mathbf{d}}_0 = \arg \min_{\tilde{\mathbf{d}}} \left| \frac{r_0}{\tilde{d}_0} \right|^2 + \left| \frac{r_1}{\tilde{d}_1} \right|^2 + \dots + \left| \frac{r_{\mathcal{K}-1}}{\tilde{d}_{\mathcal{K}-1}} \right|^2 - \frac{r_0 r_1}{\tilde{d}_0 \tilde{d}_1^*} - \frac{r_0 r_1}{\tilde{d}_0^* \tilde{d}_1} - \dots - \frac{r_{\mathcal{K}-2} r_{\mathcal{K}-1}}{\tilde{d}_{\mathcal{K}-2} \tilde{d}_{\mathcal{K}-1}^*} - \frac{r_{\mathcal{K}-2} r_{\mathcal{K}-1}}{\tilde{d}_{\mathcal{K}-2}^* \tilde{d}_{\mathcal{K}-1}}. \quad (21)$$

For BPSK,  $\left| r_v / \tilde{d}_v \right|^2 = |r_v|^2$ , which is a constant term with respect to the maximization process in (21), and thus, they can be dropped. Therefore, the detector is reduced to

$$\hat{\mathbf{d}}_0 = \arg \max_{\tilde{\mathbf{d}}_0} \sum_{v=0}^{\mathcal{K}-2} \Re \left\{ \frac{r_v r_{\hat{v}}}{\tilde{d}_v \tilde{d}_{\hat{v}}} \right\}. \quad (22)$$

Given that the pilot symbol is placed in the first subcarrier and noting that  $d_v \in \{-1, 1\}$ , then  $\tilde{d}_0 = 1$  and  $\hat{\mathbf{d}}_0$  can be written as

$$\hat{\mathbf{d}}_0 = \arg \max_{\tilde{\mathbf{d}}_0 \neq \mathbf{d}_0} \frac{1}{\tilde{d}_1} \Re \{r_0 r_1\} + \sum_{v=1}^{\mathcal{K}-2} \frac{1}{\tilde{d}_v \tilde{d}_{\hat{v}}} \Re \{r_v r_{\hat{v}}\}. \quad (23)$$

The sequence error probability ( $P_S$ ), conditioned on the channel frequency response over the  $\mathcal{K}$  symbols ( $\mathbf{H}_0$ ) and the transmitted data sequence  $\mathbf{d}_0$  can be defined as,

$$P_S |_{\mathbf{H}_0, \mathbf{d}_0} \triangleq \Pr \left( \hat{\mathbf{d}}_0 \neq \mathbf{d}_0 \right) \Big|_{\mathbf{H}_0, \mathbf{d}_0} \quad (24)$$

which can be also written in terms of the conditional probability of correct detection  $P_C$  as,

$$P_C |_{\mathbf{H}_0, \mathbf{d}_0} = 1 - \Pr \left( \hat{\mathbf{d}}_0 = \mathbf{d}_0 \right) \Big|_{\mathbf{H}_0, \mathbf{d}_0}. \quad (25)$$

Without loss of generality, we assume that  $\mathbf{d}_0 = [1, 1, \dots, 1] \triangleq \mathbf{1}$ . Therefore,

$$P_C |_{\mathbf{H}_0, \mathbf{1}} = \Pr \left( \sum_{v=0}^{\mathcal{K}-2} \Re \{r_v r_{\hat{v}}\} = \max_{\tilde{\mathbf{d}}_0} \left\{ \sum_{v=0}^{\mathcal{K}-2} \frac{\Re \{r_v r_{\hat{v}}\}}{\tilde{d}_v \tilde{d}_{\hat{v}}} \right\} \right). \quad (26)$$

Since  $\mathbf{d}_0$  has  $\mathcal{K}-1$  data symbols, then there are  $2^{\mathcal{K}-1}$  trial sequences,  $\tilde{\mathbf{d}}_0^{(0)}, \tilde{\mathbf{d}}_0^{(1)}, \dots, \tilde{\mathbf{d}}_0^{(\psi)}$ , where  $\psi = 2^{\mathcal{K}-1} - 1$ , and  $\tilde{\mathbf{d}}_0^{(\psi)} = [1, 1, \dots, 1]$ . The first symbol in every sequence is set to 1, which is the pilot symbol. By defining  $\sum_{v=0}^{\mathcal{K}-2} \frac{\Re \{r_v r_{\hat{v}}\}}{\tilde{d}_v \tilde{d}_{\hat{v}}} \triangleq A_n$ , where  $\tilde{d}_v \tilde{d}_{\hat{v}} \in \tilde{\mathbf{d}}_0^{(n)}$ , then (26) can be written as,

$$P_C |_{\mathbf{H}_0, \mathbf{1}} = \Pr (A_\psi > A_{\psi-1}, A_{\psi-2}, \dots, A_0) \quad (27)$$

which, as depicted in Appendix I, can be simplified to

$$P_C|_{\mathbf{H}_0, \mathbf{1}} = \prod_{v=0}^{\mathcal{K}-2} \Pr(\Re\{r_v r_{\acute{v}}\} > 0). \quad (28)$$

To evaluate  $P_C|_{\mathbf{H}_0, \mathbf{1}}$  given in (28), it is necessary to compute  $\Pr(\Re\{r_v r_{\acute{v}}\} > 0)$ , which can be written as

$$\Pr(\Re\{r_v r_{\acute{v}}\} > 0) = \Pr\left(\underbrace{r_v^I r_{\acute{v}}^I - r_v^Q r_{\acute{v}}^Q}_{r_{v, \acute{v}}^{\text{SP}}} > 0\right). \quad (29)$$

Given that  $\mathbf{d}_0 = [1, 1, \dots, 1]$ , then  $r_v^I = \Re\{r_v\} = H_v^I + w_v^I$  and  $r_v^Q = \Im\{r_v\} = H_v^Q + w_v^Q$ . Therefore,  $r_v^I$ ,  $r_v^Q$ ,  $r_{\acute{v}}^I$  and  $r_{\acute{v}}^Q$  are independent conditionally Gaussian random variables with averages  $H_v^I$ ,  $H_v^Q$ ,  $H_{\acute{v}}^I$  and  $H_{\acute{v}}^Q$ , respectively, and the variance for all elements is  $\sigma_w^2$ . To derive the PDF of  $r_{v, \acute{v}}^{\text{SP}}$ , the PDFs of  $r_v^I r_{\acute{v}}^I$  and  $r_v^Q r_{\acute{v}}^Q$  should be evaluated, where each of which corresponds to the product of two Gaussian random variables. Although the product of two Gaussian variables is not usually Gaussian, the limit of the moment-generating function of the product has Gaussian distribution. Therefore, the product of two variables  $X \sim \mathcal{N}(\mu_x, \sigma_x^2)$  and  $Y \sim \mathcal{N}(\mu_y, \sigma_y^2)$  tends to be  $\mathcal{N}(\mu_x \mu_y, \mu_x^2 \sigma_y^2 + \mu_y^2 \sigma_x^2)$  as the ratios  $\mu_x / \sigma_x$  and  $\mu_y / \sigma_y$  increase [27]. By noting that in in (29)  $E[r_y^x] = H_y^x$ ,  $x \in \{I, Q\}$  and  $y \in \{v, \acute{v}\}$  and  $\sigma_{r_y^x} = \sigma_w$ , thus  $E[r_y^x] / \sigma_{r_y^x} \gg 1 \forall \{x, y\}$ . Moreover, because the PDF of the sum/difference of two Gaussian random variables is also Gaussian, then,

$$r_{v, \acute{v}}^{\text{SP}} \sim \mathcal{N}(\bar{\mu}_{\text{SP}}, \bar{\sigma}_{\text{SP}}^2)$$

where

$$\bar{\mu}_{\text{SP}} = H_v^I H_{\acute{v}}^I + H_v^Q H_{\acute{v}}^Q \quad (30)$$

and

$$\bar{\sigma}_{\text{SP}}^2 = \sigma_w^2 (|H_v|^2 + |H_{\acute{v}}|^2 + \sigma_w^2). \quad (31)$$

Consequently,

$$\begin{aligned} P_C|_{\mathbf{H}_0, \mathbf{1}} &= \prod_{v=0}^{\mathcal{K}-2} \Pr(r_{v, \acute{v}}^{\text{SP}} > 0) \\ &= \prod_{v=0}^{\mathcal{K}-2} \left[ 1 - Q\left(\sqrt{\frac{2\bar{\mu}_{\text{SP}}}{\bar{\sigma}_{\text{SP}}^2}}\right) \right] \end{aligned} \quad (32)$$

and

$$P_S|_{\mathbf{H}_0, \mathbf{1}} = 1 - \prod_{v=0}^{\mathcal{K}-2} \left[ 1 - Q\left(\sqrt{\frac{2\bar{\mu}_{\text{SP}}}{\bar{\sigma}_{\text{SP}}^2}}\right) \right] \quad (33)$$

where  $Q(x) \triangleq \frac{1}{\sqrt{2\pi}} \int_x^\infty \exp\left(-\frac{t^2}{2}\right) dt$ . Since  $H_v^I$  and  $H_v^Q$  are independent, then, the condition on  $\mathbf{H}_0$  in (33) can be removed by averaging  $P_S$  over the PDF of  $\mathbf{H}_0^I$  and  $\mathbf{H}_0^Q$  as,

$$\text{SEP}|_{d=1} = \underbrace{\int_{-\infty}^{\infty} \int_{-\infty}^{\infty} \cdots \int_{-\infty}^{\infty}}_{2\mathcal{K} \text{ fold}} \text{SEP}|_{\mathbf{H}_0, d=1} f_{\mathbf{H}_0^I}(H_0^I, H_1^I, \dots, H_{\mathcal{K}-1}^I) \times \\ f_{\mathbf{H}_0^Q}(H_0^Q, H_1^Q, \dots, H_{\mathcal{K}-1}^Q) dH_0^I dH_1^I \dots dH_{\mathcal{K}-1}^I dH_0^Q dH_1^Q \dots dH_{\mathcal{K}-1}^Q \quad (34)$$

where the PDFs in (34) are multivariate Gaussian distributions that can be expressed as [28],

$$f_{\mathbf{X}}(X_0, X_1, \dots, X_{\mathcal{K}-1}) = \frac{\exp\left(-\frac{1}{2}(\mathbf{X} - \boldsymbol{\mu})^T \boldsymbol{\Sigma}^{-1}(\mathbf{X} - \boldsymbol{\mu})\right)}{\sqrt{(2\pi)^{\mathcal{K}} |\boldsymbol{\Sigma}|}} \quad (35)$$

where  $\boldsymbol{\mu}$  is the mean vector, which is defined as,

$$\boldsymbol{\mu} = \text{E}[\mathbf{X}] = [\text{E}[X_1], \text{E}[X_2], \dots, \text{E}[X_{\mathcal{K}-1}]]^T \quad (36)$$

and  $\boldsymbol{\Sigma}$  is the covariance matrix that is defined as,

$$\boldsymbol{\Sigma} = \text{E}\left[(\mathbf{X} - \boldsymbol{\mu})(\mathbf{X} - \boldsymbol{\mu})^T\right]. \quad (37)$$

Due to the difficulty of evaluating  $2\mathcal{K}$  integrals, we consider the special case of flat fading, which implies that  $H_v = H_v \triangleq H$  and  $(H^I)^2 + (H^Q)^2 \triangleq \alpha^2$ , where  $\alpha$  is the channel fading envelope,  $\alpha = |H|$ . Therefore, the SEP expression in (33) becomes,

$$P_S|_{\alpha, 1} = 1 - \left[1 - Q\left(\sqrt{\frac{\alpha^2}{\sigma_w^2(\alpha^2 + \sigma_w^2)}}\right)\right]^{\mathcal{K}-1}. \quad (38)$$

Recalling the Binomial Theorem, we get

$$(a + b)^n = \sum_{v=0}^n \binom{n}{v} a^{n-v} b^v \quad (39)$$

where,

$$\binom{n}{v} \triangleq \frac{n!}{(n-v)!v!}. \quad (40)$$

Then the SEP formula in (38) using the Binomial Theorem in (39) can be written as,

$$P_S|_{\alpha, 1} = 1 - \sum_{v=0}^{\mathcal{K}-1} \binom{\mathcal{K}-1}{v} (-1)^v \left[Q\left(\sqrt{\frac{\alpha^2}{\sigma_w^2(\alpha^2 + \sigma_w^2)}}\right)\right]^v. \quad (41)$$

The conditioning on  $\alpha$  can be removed by averaging over the PDF of  $\alpha$ , which is Rayleigh,

$$f(\alpha) = \frac{\alpha}{\sigma_H^2} e^{-\frac{\alpha^2}{2\sigma_H^2}}. \quad (42)$$

And hence,

$$P_S|_{\mathbf{1}} = \int_0^\infty P_S|_{\alpha, \mathbf{1}} f(\alpha) d\alpha. \quad (43)$$

Because the expression in (38) contains high order of  $Q$ -function  $Q^n(x)$ , evaluating the integral analytically becomes intractable for  $\mathcal{K} > 2$ . For the spacial case of  $\mathcal{K} = 2$ ,  $P_S$  can be evaluated by substituting (41) and (42) into (43) and evaluating the integral yields the following simple expression,

$$P_S|_{\mathbf{1}} = \frac{1}{2(\bar{\gamma}_s + 1)} \quad (44)$$

where  $\bar{\gamma}_s$  is the average signal-to-noise ratio (SNR),  $\bar{\gamma}_s \triangleq \frac{E[|d_v|^2]E[|H|^2]}{2\sigma_w^2}$ . Moreover, because all data sequences have equal probability of error, then  $P_S|_{\mathbf{1}} = P_S$ , which also equivalent to the bit error rate (BER). It is interesting to note that (44) is similar to the BER of the differential binary phase shift keying (DBPSK) [28]. However, the two techniques are essentially different as  $D^3$  does not require differential encoding, has no constraints on the shape of the signal constellation, and performs well even in frequency-selective fading channels.

To evaluate  $P_S$  for  $\mathcal{K} > 2$ , we use an approximation for  $Q(x)$  in [29], which is given by

$$Q(x) \approx \frac{1}{\sqrt{2\pi}(x^2 + 1)} e^{-\frac{1}{2}x^2}, \quad x \in [0, \infty). \quad (45)$$

Therefore, by substituting (45) into the conditional SEP (41) and averaging over the Rayleigh PDF (42), the evaluation of the SEP becomes straightforward. For example, evaluating the integral for  $\mathcal{K} = 3$  gives,

$$P_S|_{\mathbf{1}} = \frac{\zeta_1}{\pi} \text{Ei}(1, \zeta_1 + 1) e^{\zeta_1 + 1} \quad (46)$$

where  $\zeta_1 \triangleq \frac{1}{2\bar{\gamma}_s} \left( \frac{1}{\bar{\gamma}_s} + 1 \right)$ , and  $\text{Ei}(x)$  is the exponential integral (EI),  $\text{Ei}(x) \triangleq -\int_{-x}^\infty \frac{e^{-t}}{t} dt$ . Similarly,  $P_S$  for  $\mathcal{K} = 7$  can be evaluated to,

$$P_S|_{\mathbf{1}} = \frac{\zeta_2}{64\pi^3} [e^{\zeta_2 + 3} (2\zeta_2 + 6)^2 \text{Ei}(1, \zeta_2 + 3) - 4(\zeta_2 + 1)] \quad (47)$$

where  $\zeta_2 \triangleq \frac{1}{2\bar{\gamma}_s} \left( \frac{1}{4\bar{\gamma}_s} + 1 \right)$ .

Although the SEP is very useful indicator for the system error probability performance, the BER is actually more informative. For a sequence that contains  $\mathcal{K}_D$  information bits, the BER can be expressed as  $P_B = \frac{1}{\Lambda} P_S$ , where  $\Lambda$  denotes the average number of bit errors given a sequence error, which can be defined as

$$\Lambda = \sum_{m=1}^{\mathcal{K}_D} m \Pr(m). \quad (48)$$

Because the SEP is independent of the transmitted data sequence, then, without loss of generality, we assume that the transmitted data sequence is  $\mathbf{d}_0^{(0)}$ . Therefore,

$$\Lambda = \sum_{m=1}^{\mathcal{K}_D} m \Pr \left( \left\| \hat{\mathbf{d}}_0 \right\|^2 = m \right) \quad (49)$$

where  $\left\| \hat{\mathbf{d}}_0 \right\|^2$  in this case corresponds to the hamming weight of the detected sequence  $\hat{\mathbf{d}}_0$ , which can be expressed as

$$\Pr \left( \left\| \hat{\mathbf{d}}_0 \right\|^2 = m \right) = \Pr \left( \mathbf{d}_0^{(0)} \rightarrow \bigcup_i \mathbf{d}_0^{(i)}, \left\| \mathbf{d}_0^{(i)} \right\|^2 = m \right) \quad (50)$$

where  $\mathbf{d}_0^{(0)} \rightarrow \mathbf{d}_0^{(i)}$  denotes the pairwise error probability (PEP). By noting that  $\Pr \left( \mathbf{d}_0^{(0)} \rightarrow \mathbf{d}_0^{(i)} \right) \neq \Pr \left( \mathbf{d}_0^{(0)} \rightarrow \mathbf{d}_0^{(j)} \right) \forall i \neq j$ , then deriving the PEP for all cases of interest is intractable. As an alternative, a simple approximation is derived.

For a sequence that consists of  $\mathcal{K}_D$  information bits, the BER is bounded by

$$\frac{1}{\mathcal{K}_D} P_S \leq P_B \leq P_S. \quad (51)$$

In practical systems, the number of bits in the detected sequence is generally not too large, which implies that the upper and lower bounds in (51) are relatively tight, and hence, the BER can be approximated as the middle point between the two bounds as,

$$P_B \approx \frac{P_S}{0.5(1 + \mathcal{K}_D)}. \quad (52)$$

The analysis of the general  $1 \times \mathcal{N}$  SIMO system is straightforward extension of the single-input single-output (SISO) case. To simplify the analysis, we consider the flat channel case where the conditional SEP can be written as,

$$P_S |_{\alpha} = 1 - \left[ 1 - Q \left( \sqrt{\frac{\sum_{i=1}^{\mathcal{N}} \alpha_i^2}{\sigma_w^2 (\mathcal{N} \sigma_w^2 + \sum_{i=1}^{\mathcal{N}} \alpha_i^2)}} \right) \right]^{\mathcal{K}-1}. \quad (53)$$

Given that all the receiving branches are independent, the fading envelopes will have Rayleigh distribution  $\alpha_i \sim \mathcal{R}(2\sigma_H^2) \forall i$ , and thus,  $\sum_{i=1}^{\mathcal{N}} \alpha_i^2 \triangleq a$  will have Gamma distribution,  $a \sim \mathcal{G}(\mathcal{N}, 2\sigma_H^2)$ ,

$$f(a) = (2\sigma_H^2)^{\mathcal{N}} e^{-2\sigma_H^2 a} \frac{a^{\mathcal{N}-1}}{\Gamma(\mathcal{N})}. \quad (54)$$

Therefore, the unconditional SEP can be evaluated as,

$$P_S = \int_0^{\infty} P_S |_{\alpha} f_A(a) da. \quad (55)$$

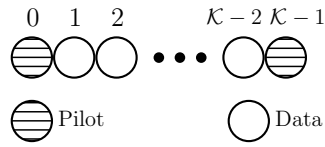


Fig. 4. Double-sided pilot segment.

For the special case of  $\mathcal{N} = 2$ ,  $\mathcal{K} = 2$ ,  $P_S$  can be evaluated as,

$$P_S = \frac{1}{2} + Q\left(\frac{\varkappa}{\sqrt{\bar{\gamma}_s}}\right) \left[ 2\bar{\gamma}_s \left( \frac{\bar{\gamma}_s}{\sqrt{2}} + 2 \right) - e^{\varkappa^2} \right] - \bar{\gamma}_s \frac{\varkappa}{\sqrt{2\pi}} \quad (56)$$

where  $\varkappa \triangleq \sqrt{2 + \bar{\gamma}_s}$ . Computing the closed-form formulas for other values of  $\mathcal{N}$  and  $\mathcal{K}$  can be evaluated following the same approach used in the SISO case.

### B. Double-Sided Pilot

Embedding more pilots in the detection segment can improve the detector's performance. Consequently, it worth investigating the effect of embedding more pilots in the SEP analysis. More specifically, we consider double-sided segment,  $\tilde{d}_0 = 1$ ,  $\tilde{d}_{\mathcal{K}-1} = 1$ , as illustrated in Fig. 4. In this case, the detector can be expressed as,

$$\hat{\mathbf{d}}_0 = \arg \max_{\tilde{\mathbf{d}}_0} \frac{1}{\tilde{d}_1} \Re\{r_0 r_1\} + \frac{1}{\tilde{d}_{\mathcal{K}-2}} \Re\{r_{\mathcal{K}-2} r_{\mathcal{K}-1}\} + \sum_{v=1}^{\mathcal{K}-3} \frac{1}{\tilde{d}_v \tilde{d}_v} \Re\{r_v r_v\}, \quad \mathcal{K} \in \{3, 4, \dots, N-1\}. \quad (57)$$

From the definition in (57), the probability of receiving the correct sequence can be derived based on the reduced number of trials as compared to (23). Therefore,

$$P_{C|\mathbf{H}_{0,1}} = \Pr\left( (\Re\{r_0 r_1\} + \Re\{r_{\mathcal{K}-2} r_{\mathcal{K}-1}\}) \cap \Re\{r_1 r_2\} \cap \Re\{r_2 r_3\} \cap \dots \cap \Re\{r_{\mathcal{K}-4} r_{\mathcal{K}-3}\} > 0 \right) \quad (58)$$

which, similar to the single-sided case, can be written as,

$$P_{C|\mathbf{H}_{0,1}} = \Pr\left( \left[ \prod_{v=0}^{\mathcal{K}-3} \Pr(\Re\{r_v r_v\}) + \prod_{v=1}^{\mathcal{K}-2} \Pr(\Re\{r_v r_v\}) \right] > 0 \right). \quad (59)$$

Therefore,

$$P_{S|\mathbf{H}_{0,1}} = 1 - \left[ 1 - Q\left( \sqrt{\frac{2\sqrt{2}\bar{\mu}_{\text{SP}}}{\bar{\sigma}_{\text{SP}}^2}} \right) \right] \times \prod_{v=1}^{\mathcal{K}-3} \left[ 1 - Q\left( \sqrt{\frac{2\bar{\mu}_{\text{SP}}}{\bar{\sigma}_{\text{SP}}^2}} \right) \right]. \quad (60)$$



For flat fading channels, the SEP expression in (60) can be simplified by following the same procedure in Subsection V-A, for the special case of  $\mathcal{K} = 3$ , the SEP becomes,

$$P_S = \left( \frac{\Upsilon}{2} - \sqrt{2} \right) \frac{1}{\Upsilon} \quad (61)$$

where  $\Upsilon \triangleq \sqrt{8\bar{\gamma}_s + \sqrt{2} \left( 4 + \frac{1}{\bar{\gamma}_s} \right)}$ . For  $\mathcal{K} > 3$ , the approximation of  $Q^n(x)$ , as illustrated in Subsection V-A, can be used in (60) to average of the PDF in (42). For example, the case  $\mathcal{K} = 4$  can be evaluated as,

$$P_S = \frac{1}{8\pi\bar{\gamma}_s} (\Omega_1 - 1) e^{\Omega_1} \text{Ei}(1, \Omega_1) \quad (62)$$

where  $\Omega_1 \triangleq 1 + \frac{\sqrt{2}}{4\bar{\gamma}_s} \left( 1 + \frac{1}{4\bar{\gamma}_s} \right)$ . For  $\mathcal{K} = 6$ ,

$$P_S = \frac{\Omega_1 - 1}{4\pi^2} \left[ 1 - [(\Omega_1 - 1) e^{\Omega_2} + 2] \text{Ei}(1, \Omega_2) \right] \quad (63)$$

where  $\Omega_2 \triangleq 2 + \frac{\sqrt{2}}{\bar{\gamma}_s} \left( 8 + \frac{1}{32\bar{\gamma}_s} \right)$ . For the double-sided pilot,  $P_B = P_S$  for the case of  $\mathcal{K} = 3$ , while it can be computed using (52) for  $\mathcal{K} > 3$ .

### C. Pilots Power Boosting

In most practical wireless standards such as LTE and LTE-A [4], pilots can be allocated extra power to improve the channel estimation accuracy, and hence, reduce the error rate. Likewise, allocating extra power to pilot symbols in the  $D^3$  as described in Subsections V-A and V-B can enhance the SEP performance, particularly for frequency-selective channels. To address this parameter in the analysis, the conditional SEP for the single-sided pilot system is modified to,

$$\begin{aligned} P_{S|\mathbf{H}_{0,1}} &= 1 - \Pr(\Re\{r_{0,1}^{\text{SP}}\} > 0) \prod_{v=0}^{\mathcal{K}-3} \Pr(\Re\{r_{v,\hat{v}}^{\text{SP}}\} > 0) \\ &= \left[ 1 - Q \left( \sqrt{\frac{\bar{\mu}_{\text{SP}}(1+\mathcal{P})}{\bar{\sigma}_{\text{SP}}^2}} \right) \right] \times \prod_{v=0}^{\mathcal{K}-3} \left[ 1 - Q \left( \sqrt{\frac{2\bar{\mu}_{\text{SP}}}{\bar{\sigma}_{\text{SP}}^2}} \right) \right] \end{aligned} \quad (64)$$

where  $\mathcal{P}$  is the additional power allocated to the pilots. And for the double-sided pilot,

$$P_{S|\mathbf{H}_{0,1}} = 1 - \left[ 1 - Q \left( \sqrt{8} \sqrt{\frac{\bar{\mu}_{\text{SP}}}{\bar{\sigma}_{\text{SP}}^2}} \mathcal{P} \right) \right] \times \prod_{v=1}^{\mathcal{K}-3} \left[ 1 - Q \left( \sqrt{\frac{2\bar{\mu}_{\text{SP}}}{\bar{\sigma}_{\text{SP}}^2}} \right) \right] \quad (65)$$

Finally, finding the closed-form formulas follows the same steps discussed in subsections V-A and V-B. However, the obtained formulae are omitted due to the space limitations.

## VI. COMPLEXITY ANALYSIS

The computational complexity is evaluated as the total number of primitive operations needed to perform the detection. The operations that will be used are the number of real additions ( $R_A$ ), real multiplications ( $R_M$ ), and real divisions ( $R_D$ ) required to produce the set of detected symbols  $\hat{\mathbf{d}}$  for each technique. It worth noting that one complex multiplication ( $C_M$ ) is equivalent to four  $R_M$  and three  $R_A$  operations, while one complex addition ( $R_A$ ) requires two  $R_A$ . In this analysis, we assume that constant modulus (CM) constellations such as MPSK is used, and hence, the evaluation of the complexity analysis is shown in the two following subsections.

### A. Complexity of Conventional OFDM Detectors

The complexity of the conventional OFDM receiver that consists of the following main steps with the corresponding computational complexities:

- 1) Channel estimation of the pilot symbols, which computes  $\hat{H}_k$  at all pilot subcarriers. Assuming that the pilot symbol  $d_k$  is selected from a CM constellation, then  $\hat{H}_k = r_k d_k^*$  and hence,  $N_P$  complex multiplications are required. Therefore,  $R_A^{(1)} = 4N_P$  and  $R_M^{(1)} = 4N_P$ .
- 2) Interpolation, which is used to estimate the channel at the non-pilot subcarriers. The complexity of the interpolation process depends on the interpolation algorithm used. For comparison purposes, we assume that linear interpolation is used, which is the least complex interpolation algorithm. The linear interpolation requires one complex multiplication and two complex additions per interpolated sample. Therefore, the number of complex multiplications required is  $N - N_P$  and the number of complex additions is  $2(N - N_P)$ . And hence,  $R_A^{(2)} = 7(N - N_P)$  and  $R_M^{(2)} = 4(N - N_P)$ .
- 3) Equalization, a single-tap equalizer requires  $N - N_P$  complex division to compute the decision variables  $\check{r}_k = \frac{r_k}{\hat{H}_k} = r_k \frac{\hat{H}_k^*}{|\hat{H}_k^*|^2}$ . Therefore, one complex division requires two complex multiplications and one real division. Therefore,  $R_A^{(3)} = 6(N - N_P)$ ,  $R_M^{(3)} = 8(N - N_P)$  and  $R_D^{(3)} = (N - N_P)$ .
- 4) Detection, assuming symbol-by-symbol minimum distance detection, the detector can be expressed as  $\hat{d}_k = \arg \min_{\tilde{d}_i} J(\tilde{d}_i)$ ,  $\forall i \in \{0, 1, \dots, M - 1\}$  where  $J(\tilde{d}_i) = |\check{r}_k - \tilde{d}_i|^2$ . Assuming CM modulation is used, expanding the cost function and dropping the constant terms we can write  $J(\tilde{d}_i) = -\check{r}_k \tilde{d}_i^* - \check{r}_k^* \tilde{d}_i$ . We can also drop the minus sign from the cost function, and thus, the objective becomes maximizing the cost function  $\hat{d}_k =$

$\arg \min_{\tilde{d}_i} J(\tilde{d}_i)$ . Since the two terms are complex conjugate pair, then  $-\check{r}_k \tilde{d}_k^* - \check{r}_k^* \tilde{d}_k = 2\Re\{\check{r}_k \tilde{d}_k^*\}$ , and thus we can write the detected symbols as,

$$\hat{d}_k = \arg \max_{\tilde{d}_k} \left( \Re\{\check{r}_k\} \Re\{\tilde{d}_k^*\} - \Im\{\check{r}_k\} \Im\{\tilde{d}_k^*\} \right) \quad (66)$$

Therefore, the number of real multiplications required for each information symbol is  $2M$ , and the number of additions is  $M$ . Therefore,  $R_A^{(4)} = (N - N_P)M$  and  $R_M^{(4)} = 2(N - N_P)M$ .

Finally, the total computational complexity per OFDM symbol can be obtained by adding the complexities of the individual steps 1  $\rightarrow$  4, as:

$$R_A = \sum_{i=1}^4 R_A^{(i)} = (13 + M)N - (10 + M)N_P \quad (67)$$

$$R_M = \sum_{i=1}^4 R_M^{(i)} = 2N(6 + M) - 2N_P(4 + M) \quad (68)$$

$$R_D = \sum_{i=1}^4 R_D^{(i)} = N - N_P. \quad (69)$$

### B. Complexity of the $D^3$

The complexity of the  $D^3$  based on the Viterbi algorithm is mostly determined by the branch and path metrics calculation. The branch metrics can be computed as

$$J_{m,n}^c = \frac{|r_c|^2}{|\tilde{d}_m|^2} - \frac{r_c r_{c+1}^*}{\tilde{d}_m \tilde{d}_n^*} - \frac{r_c^* r_{c+1}}{\tilde{d}_m^* \tilde{d}_n} + \frac{|r_c|^2}{|\tilde{d}_n|^2}. \quad (70)$$

For CM constellation, the first and last terms are constants, and hence, can be dropped. Therefore,

$$J_{m,n}^c = -\frac{r_c r_{c+1}^*}{\tilde{d}_m \tilde{d}_n^*} + \frac{r_c^* r_{c+1}}{\tilde{d}_m^* \tilde{d}_n}. \quad (71)$$

By noting that the two terms in (71) are the complex conjugate pair, then

$$J_{m,n}^c = -2\Re\left\{\frac{r_c r_{c+1}^*}{\tilde{d}_m \tilde{d}_n^*}\right\}. \quad (72)$$

From the expression in (72), the constant “ $-2$ ” can be dropped from the cost function, however, the problem will be flipped to a maximization problem. Therefore, by expanding (72), we get,

$$J_{m,n}^c = \Re\left\{\frac{\Re\{r_c\} \Re\{r_{c+1}^*\} - \Im\{r_c\} \Im\{r_{c+1}^*\} + j[-\Re\{r_c\} \Im\{r_{c+1}^*\} + \Im\{r_c\} \Re\{r_{c+1}^*\}]}{\Re\{\tilde{d}_m \tilde{d}_n^*\} + j\Im\{\tilde{d}_m \tilde{d}_n^*\}}\right\}. \quad (73)$$

By defining  $\tilde{d}_m \tilde{d}_n^* \triangleq \tilde{u}_{m,n}$ , and using complex numbers identities, we get (74),

$$J_{m,n}^c = \frac{[\Re\{r_c\} \Re\{r_c^*\} + \Im\{r_c\} \Im\{r_c^*\}] \Re\{\tilde{u}_{m,n}\} - [-\Re\{r_c\} \Im\{r_c^*\} + \Im\{r_c\} \Re\{r_c^*\}] \Im\{\tilde{u}_{m,n}\}}{\Re\{\tilde{u}_{m,n}\}^2 + \Im\{\tilde{u}_{m,n}\}^2}. \quad (74)$$

For CM,  $\Re\{\tilde{u}_{m,n}\}^2 + \Im\{\tilde{u}_{m,n}\}^2$  is constant, and hence, it can be dropped from the cost function as,

$$J_{m,n}^c = [\Re\{r_c\} \Re\{r_{c+1}^*\} + \Im\{r_c\} \Im\{r_{c+1}^*\}] \Re\{\tilde{u}_{m,n}\} - [-\Re\{r_c\} \Im\{r_{c+1}^*\} + \Im\{r_c\} \Re\{r_{c+1}^*\}] \Im\{\tilde{u}_{m,n}\}. \quad (75)$$

To compute  $J_{m,n}^c$ , it is worth noting that the two terms in brackets are independent of  $\{m, n\}$ , and hence, they are computed only once for each value of  $c$ . Therefore, the complexity at each step in the trellis can be computed as  $R_A = 3 \times 2^M$ ,  $R_M = 4 + 2 \times 2^M$  and  $R_D = 0$ , where  $2^M$  is the number of branches at each step in the trellis. However, if the trellis starts or ends by a pilot, then only  $M$  computations are required. By noting that the number of full steps is  $N - 2N_P - 1$ , and the number of steps that require  $M$  computations is  $2(N_P - 1)$ , then the total computations of the branch metrics (BM) are:

$$R_A^{BM} = (3 \times 2^M) (N - 2N_P - 1) + 2(3 \times M) (N_P - 1)$$

$$R_M^{BM} = (4 + 2^{M+1}) (N - 2N_P - 1) + 2(N_P - 1) (4 + 2M)$$

$$R_D^{BM} = 0$$

The path metrics (PM) require  $R_A^{PM} = (N - 2N_P - 1) + M(N_P - 1)$  real addition. Therefore, the total complexity is:

$$R_A = (N - 2N_P - 1) (5 \times 2^M) + 7M (N_P - 1) \quad (76)$$

$$R_M = (N - 2N_P - 1) (4 + 2^{M+1}) + 2(N_P - 1) (4 + 2M) \quad (77)$$

$$R_D = 0 \quad (78)$$

To compare the complexity of the  $D^3$  with the conventional detector using LS channel estimation, linear interpolation, zero-forcing (ZF) equalization and MLD. The relative complexity is denoted by  $\eta$ , which corresponds to the ratio of the  $D^3$  complexity to the conventional detector, i.e.,  $\eta(R_A)$  denotes the ratio of real additions and  $\eta(R_M)$  corresponds to the ratio of real multiplications. As depicted in Table I,  $R_A$  and  $R_M$  of the  $D^3$  is about 75% of the conventional detector. It is worth

TABLE I  
COMPUTATIONAL COMPLEXITY COMPARISON USING DIFFERENT VALUES OF  $N$ ,  $N_P = N/4$ .

$N$	128	256	512	1024	2048
$\eta(R_A)$ %	73.4	74.2	74.6	74.8	74.9
$\eta(R_M)$ %	75.2	76.0	76.5	76.7	76.8
$R_D$	96	192	384	768	1536
$\eta(CP)$ %	27.0	27.7	29.5	32.2	35.0

noting that  $R_D$  in the table corresponds to the number of divisions in the conventional OFDM since the  $D^3$  does not require any divisions operations. For a more informative comparison between the two systems, we use the computational power analysis presented in [30], where the total power for each detector is estimated based on the total number of operations. Table I shows the relative computational power  $\eta(CP)$ , which shows that the  $D^3$  detector requires only 27% CP as compared to the conventional detector for  $N = 128$ , and 35% for  $N = 2048$ .

It is worth noting that linear interpolation has lower complexity as compared to more accurate interpolation schemes such as the spline interpolation [31], [32], which comes at the expense of the error rate performance. Therefore, the results presented in Table I can be generally considered as upper bounds on the relative complexity of the  $D^3$ , when more accurate interpolation schemes are used, the relative complexity will drop even further as compared to the results in Table I.

## VII. NUMERICAL RESULTS

This section presents the performance of the  $D^3$  detector in terms of the BER under several operating scenarios. The system model follows the LTE-A physical layer (PHY) specifications [4], where the adopted OFDM symbol has  $N = 512$  subcarriers, the CP length  $N_{CP} = 64$  samples, the sampling frequency  $f_s = 7.68$  MHz, the subcarrier spacing  $\Delta f = 15$  kHz, and the pilot grid follows that of Fig. 1. The total OFDM symbol period is  $75 \mu\text{sec}$ , and CP period is  $4.69 \mu\text{sec}$ . The channel models used are the AWGN, flat Rayleigh fading channel, and the typical urban (TUx) multipath fading model [33] that consists of 6 taps with normalized delays of  $[0, 2, 3, 9, 13, 29]$  and average tap's gain of  $[0.2, 0.398, 0.2, 0.1, 0.063, 0.039]$ , which corresponds to severe frequency-selective channels. The TUx multipath fading model is also used to model a moderate frequency-selective channel where the number of taps in the channel is 9 with normalized delays of  $[0, 1, \dots, 8]$  samples, and the average taps' gains are  $[0.269, 0.174, 0.289,$

0.117, 0.023, 0.058, 0.036, 0.026, 0.008]. The channel taps are assumed to be independent and Rayleigh distributes. Monte Carlo simulations results are obtained to corroborate the analytical results for the BPSK and to evaluate the BER for higher order modulation. For each simulation run,  $10^6$  OFDM symbols are processed.

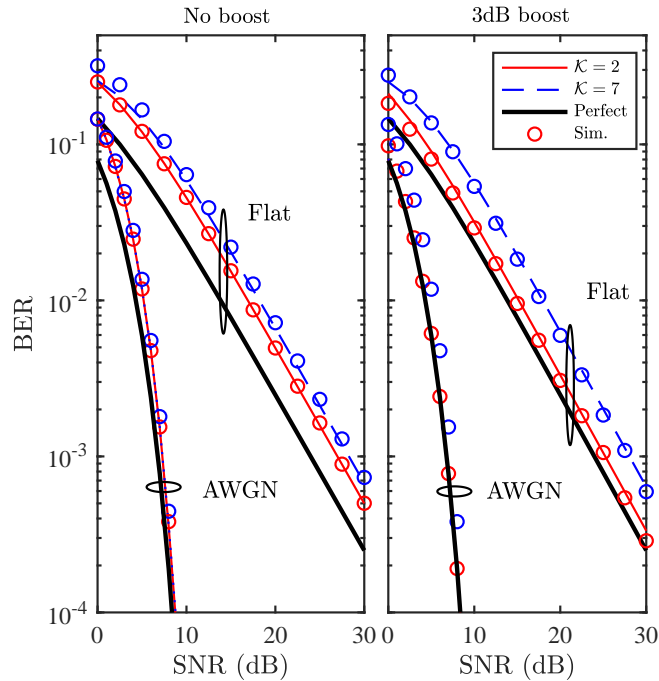


Fig. 5. Analytical and simulated BER of the  $D^3$  using the single-sided pilots for different values of  $\mathcal{K}$  over AWGN and flat fading channels using BPSK,  $\mathcal{N} = 1$ .

Fig. 5 shows the BER of the single-sided (SS) SISO- $D^3$  system over AWGN and flat fading channels for  $\mathcal{K} = 2$  and 6, and the pilots are with and without 3 dB boosting. The results show that the  $D^3$  BER is comparable to the coherent symbol-by-symbol detection with perfect CSI in the AWGN case, regardless of the value of  $\mathcal{K}$  or the pilot boost power. For the flat fading channel, the results in the figure show that the value of  $\mathcal{K}$  has more impact on the BER, particularly for the 3 dB boost case, where the BER difference between the  $\mathcal{K} = 2$  and 6 cases is about 2.8 dB at BER of  $10^{-3}$ , while it is only 1.6 dB for the case without pilot boosting. Moreover, the BER when  $\mathcal{K} = 6$  is slightly less than the BER without pilot boosting, and it is higher than the  $\mathcal{K} = 2$  for all cases. It is also worth noting that the analytical and simulation results match very well for all cases.

Fig. 6 presents the BER for the double-sided (DS) segment case, where  $\mathcal{K} = 3$  and 7. It is

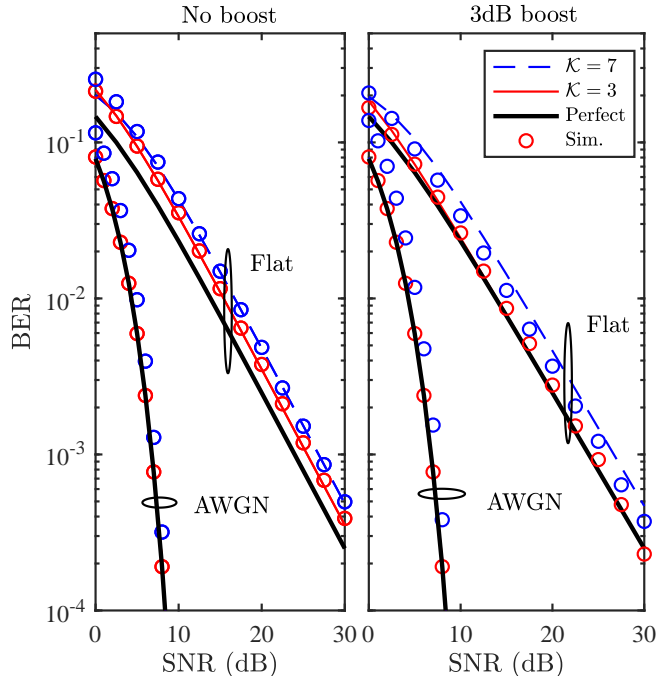


Fig. 6. BER of the SISO- $D^3$  using the double-sided segment for  $\mathcal{K} = 3$  and  $7$  over flat channels using BPSK.

worth noting that the number of data symbols  $\mathcal{K}_D = \mathcal{K} - 1$  for the single-sided and  $\mathcal{K}_D = \mathcal{K} - 2$  in the double-sided because there are two pilot symbols at both ends of the data segment. Generally speaking, the BER using the double-sided pilot segment has similar trends to the BER with the single-sided pilot except that the results for all scenarios become closer to the coherent BPSK BER with perfect CSI because having more pilots reduces the probability of having the sequence inverted due to the phase ambiguity problem. The figure shows that the analytical and simulation results match very well for all cases, which confirms the accuracy of the derived approximations.

The effect of the frequency selectivity on the SISO- $D^3$  is illustrated in Fig. 7 for the case  $\mathcal{K}_D = 1$ . As can be noted from the figure, frequency-selective channels introduce error floors at high SNRs, which is due to the difference between adjacent channel values caused by the channel frequency selectivity. Furthermore, the results show the validity of the analysis for frequency-selective channels. The analytical results are presented only for the SS where  $\mathcal{K} = 2$  because evaluating the BER for  $\mathcal{K} > 2$  becomes computationally prohibitive. For example, evaluating the integral (34) for the  $\mathcal{K} = 3$  requires solving a 6-fold integral. The results for the frequency-selective channels are quite different from the AWGN and flat fading cases. In particular, the

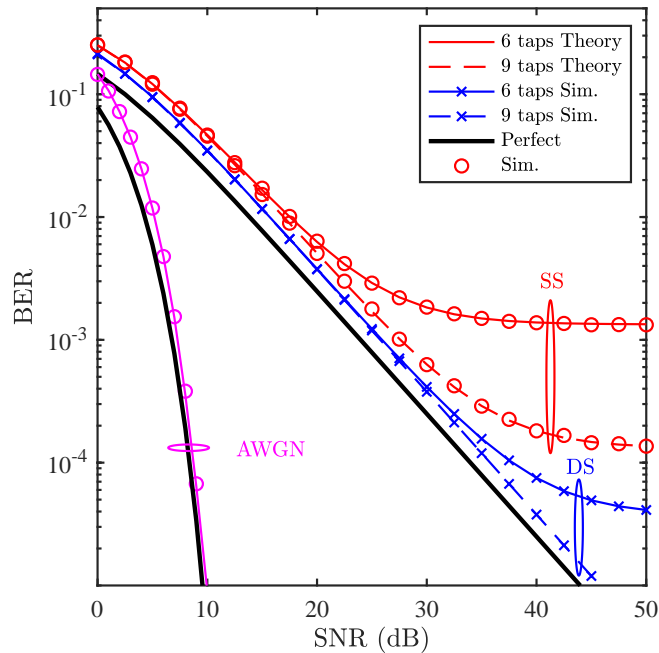


Fig. 7. Analytical and simulated BER of the proposed  $D^3$  in frequency-selective channels using BPSK,  $\mathcal{K}_D = 1$  and  $\mathcal{N} = 1$ .

BER performance drastically changes when the DS pilot segment is used. Moreover, the impact of the frequency selectivity is significant, particularly for the SS pilot case.

Fig. 8 shows the analytical and simulated BER of the  $1 \times 2$  SIMO  $D^3$  over flat fading channels for single and double-sided pilot segments without pilot boosting. It can be noted from the figure that the maximum ratio combiner (MRC) BER with perfect CSI outperforms the DS and SS systems by about 2 and 3 dB, respectively. Moreover, the figure shows that the MSDD [25] and the  $D^3$  have equivalent BER in SISO and SIMO scenarios.

Fig. 9 shows the BER of the  $D^3$ , conventional pilot-based OFDM with perfect and imperfect CSI, and the MSDD, all using BPSK. The  $D^3$  systems is implemented using the Viterbi algorithm, while the conventional OFDM coherent detector is implemented using linear and spline interpolation. As expected, the coherent OFDM with perfect CSI outperforms all the other considered schemes. Nevertheless, the imperfect CSI introduced by the channel estimation errors caused by the noise-contaminated pilots and interpolation operations harmed the BER of the coherent systems, particularly with the low complexity linear interpolation. The high complexity spline interpolation outperforms linear interpolation, but still outperformed by the



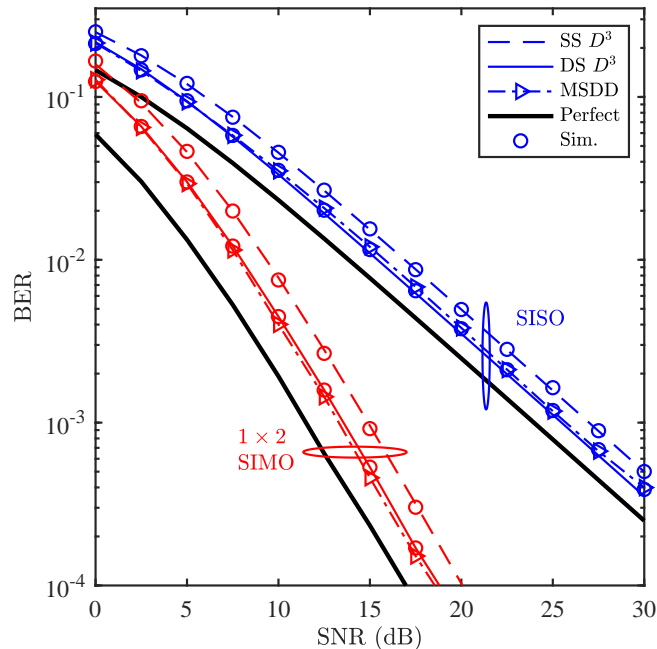


Fig. 8. BER of  $D^3$  and MSDD [25] SISO and SIMO using double-sided and single-sided pilots, flat fading, BPSK, no boosting,  $\mathcal{N} = 1, 2$ , and  $\mathcal{K}_D = 1$ .

$D^3$ . Although the MSDD managed to offer slightly better BER than the  $D^3$  at low SNRs, it suffers from a high level error floor at high SNRs because it is very sensitive to frequency-selective channels. Overall, the performance of the  $D^3$  can be considered superior because it combines low complexity reliability.

Figs. 10 shows the BER of the SISO and  $1 \times 2$  SIMO MSDD, coherent with linear and spline interpolation, and coherent with perfect CSI. For both SISO and SIMO, the BER of all the considered techniques converges because the AWGN dominates the BER. For moderate and high SNRs, the  $D^3$  outperforms all the other considered techniques, and it is about 3.5 and 2.75 dB at BER of  $10^{-3}$  from the perfect CSI case for the SISO and SIMO systems, respectively.

Fig. 11 show the BER of the  $D^3$  and the other considered systems using 16-QAM. As can be seen from the figure, the MSDD managed to slightly outperform the  $D^3$  at low SNRs, and the coherent OFDM with spline interpolation outperforms the  $D^3$  at high SNRs. However, the spline interpolation has generally high complexity.

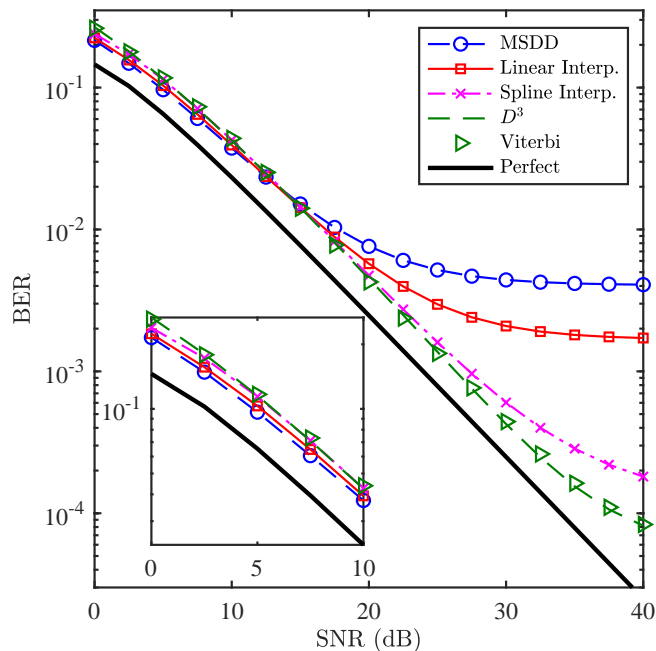


Fig. 9. BER of the double-sided SISO  $D^3$  for a complete OFDM block ( $\mathcal{K} = N$ ) over the 6-taps frequency-selective channel using BPSK, compared with MSDD [25].

### VIII. CONCLUSION

This work proposed a new receiver design for OFDM-based broadband communication systems. The new receiver performs the detection process directly from the FFT output symbols without the need of experiencing the conventional steps of channel estimation, channel interpolation, and channel equalization, which led to a massive complexity reduction. Moreover, the  $D^3$  system can be deployed efficiently using the Viterbi algorithm. With the reduced complexity, the system was analyzed theoretically and validated using simulations, which shows that it outperforms the conventional pilot-based receivers using different interpolation techniques over frequency-selective channels.

### APPENDIX I

By defining the events  $A_\psi > A_n \triangleq E_{\psi,n}$ ,  $n \in \{0, 1, \dots, \psi - 1\}$ , then,

$$P_{C|\mathbf{H}_{0,1}} = P \left( \bigcap_{n=0}^{\psi-1} E_{\psi,n} \right) \tag{79}$$

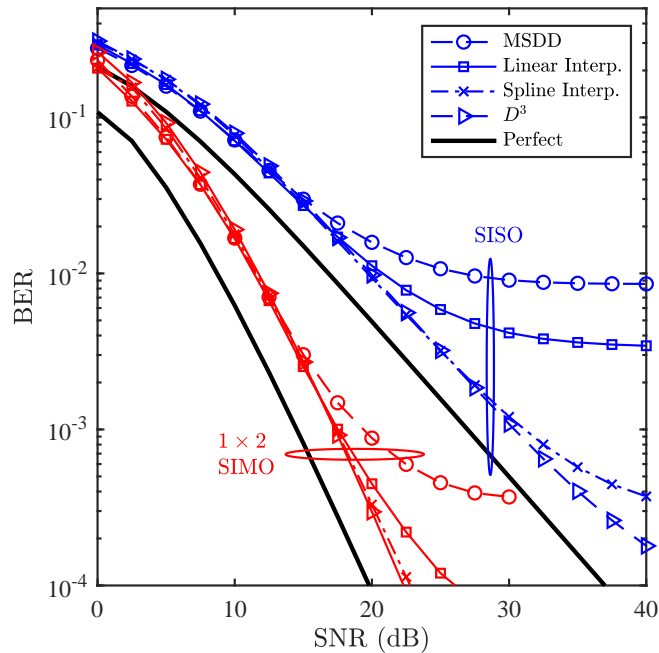


Fig. 10. BER of the double-sided SISO  $D^3$  and MSDD [25] over the 6-taps frequency-selective channel using QPSK,  $\mathcal{K}_D = 1$ ,  $\mathcal{N} = 1, 2$ .

Using the chain rule,  $P_C|_{\mathbf{H}_{0,1}}$  can be written as,

$$P_C|_{\mathbf{H}_{0,1}} = \Pr \left( E_{\psi, \psi-1} \mid \bigcap_{n=0}^{\psi-2} E_{\psi, n} \right) \Pr \left( \bigcap_{n=0}^{\psi-2} E_{\psi, n} \right). \quad (80)$$

For  $\mathcal{K} = 2$ ,  $\psi = 1$ ,  $\tilde{\mathbf{d}}_0^{(0)} = [1, -1]$ ,  $\tilde{\mathbf{d}}_0^{(1)} = [1, 1]$ , and thus,

$$\begin{aligned} P_C|_{\mathbf{H}_{0,1}} &= \Pr(E_{1,0}) \\ &= \Pr(\Re\{r_1 r_2\} > \Re\{-r_1 r_2\}) \\ &= \Pr(\Re\{r_0 r_1\} > 0) \end{aligned} \quad (81)$$

For  $\mathcal{K} = 3$ ,  $\psi = 4$ ,  $\tilde{\mathbf{d}}_0^{(0)} = [1, 1, -1]$ ,  $\tilde{\mathbf{d}}_0^{(1)} = [1, -1, -1]$ ,  $\tilde{\mathbf{d}}_0^{(2)} = [1, -1, 1]$  and  $\tilde{\mathbf{d}}_0^{(3)} = [1, 1, \dots, 1]$ . Using the chain rule

$$\begin{aligned} P_C|_{\mathbf{H}_{0,1}} &= \Pr(E_{3,2} | E_{3,1}, E_{3,0}) \Pr(E_{3,1}, E_{3,0}) \\ &= \Pr(E_{3,2} | E_{3,1}, E_{3,0}) \Pr(E_{3,1} | E_{3,0}) \Pr(E_{3,0}) \end{aligned} \quad (82)$$

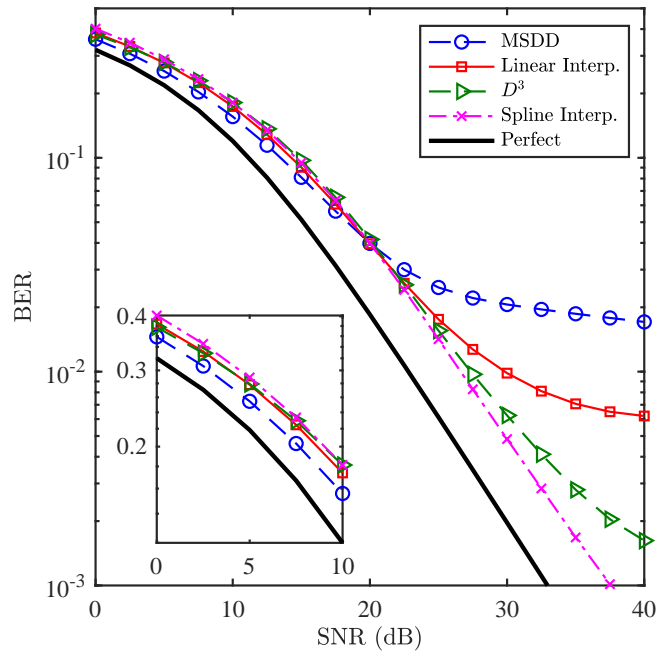


Fig. 11. BER of the double-sided SISO  $D^3$  and MSDD [25] over the 6-taps frequency-selective channel using 16-QAM,  $\mathcal{K} = 7$ .

However,  $\Pr(E_{3,0}) = \Pr(A_3 > A_0)$ , and thus

$$\begin{aligned}
 \Pr(E_{3,0}) &= \Pr(\Re\{r_0 r_1 + r_1 r_2\} > \Re\{r_0 r_1 - r_1 r_2\}) \\
 &= \Pr(\Re\{r_1 r_2\} > \Re\{-r_1 r_2\}) \\
 &= \Pr(\Re\{r_1 r_2\} > 0).
 \end{aligned} \tag{83}$$

The second term in (82) can be evaluated by noting that the events  $E_{3,1}$  and  $E_{3,0}$  are independent.

Therefore  $\Pr(E_{3,1}|E_{3,0}) = \Pr(E_{3,1})$ , which can be computed as

$$\begin{aligned}
 \Pr(E_{3,1}) &= \Pr(\Re\{r_0 r_1 + r_1 r_2\} > \Re\{-r_0 r_1 + r_1 r_2\}) \\
 &= \Pr(\Re\{r_0 r_1\} > \Re\{-r_0 r_1\}) \\
 &= \Pr(\Re\{r_0 r_1\} > 0)
 \end{aligned} \tag{84}$$

The first term in (82)  $\Pr(E_{3,2}|E_{3,1}, E_{3,0}) = 1$  because if  $A_3 > \{A_1, A_0\}$ , then  $A_3 > A_2$  as well. Consequently,

$$P_{C|H_{0,1}} = \Pr(\Re\{r_0 r_1\} > 0) \Pr(\Re\{r_1 r_2\} > 0). \tag{85}$$

By induction, it is straightforward to show that  $P_C|_{\mathbf{H}_0, \mathbf{1}}$  can be written as,

$$P_C |_{\mathbf{H}, \mathbf{d}=\mathbf{1}} = \prod_{n=0}^{\mathcal{K}-2} \Pr(\Re\{r_n r_n^*\} > 0). \quad (86)$$

## REFERENCES

- [1] Radio broadcasting systems; digital audio broadcasting (DAB) to mobile, portable and fixed receivers, ETS Std. 300 401, 1995.
- [2] Digital video broadcasting (DVB); framing structure, channel coding and modulation for digital terrestrial television, ETSI Std. EN 300744 v1.6.1, 2008.
- [3] IEEE Standard for Local and metropolitan area networks Part 16: Air Interface for Broadband Wireless Access Systems Amendment 3: Advanced Air Interface, IEEE Std. 802.16m, 2011.
- [4] LTE; Evolved Universal Terrestrial Radio Access (E-UTRA), LTE physical layer, 3GPP TS 36.300, 2011.
- [5] P. Guan et al., "5G field trials: OFDM-based waveforms and mixed numerologies," *IEEE J. Sel. Areas Commun.*, vol. 35, no. 6, pp. 1234-1243, June 2017.
- [6] Weile Zhang, Qinye Yin, Wenjie Wang, and Feifei Gao, "One-shot blind CFO and channel estimation for OFDM with multi-antenna receiver," *IEEE Trans. Signal Process.*, vol. 62, no. 15, pp. 3799-3808, Aug. 2014.
- [7] Song Noh, Youngchul Sung, Michael Zoltowski, "A new precoder design for blind channel estimation in MIMO-OFDM systems," *IEEE Trans. Wireless Commun.*, vol. 13, no. 12, pp. 7011-7024, Dec. 2014.
- [8] A. Saci, A. Al-Dweik, A. Shami, and Y. Iraqi, "One-shot blind channel estimation for OFDM systems over frequency-selective fading channels," *IEEE Trans. Commun.*, vol. 65, no. 12, pp. 5445-5458, Dec. 2017.
- [9] A. Saci, A. Al-Dweik and A. Shami, "Blind channel estimation using cooperative subcarriers for OFDM systems," *IEEE Int. Conf. Commun. (ICC)*, Kansas City, USA, May 2018.
- [10] Xiaofei Zhang and Dazhuan Xu, "Blind channel estimation for multiple antenna OFDM system subject to unknown carrier frequency offset," *Journal of Systems Engineering and Electronics.*, vol. 25, no. 5, pp. 721-727, Oct. 2014.
- [11] A. Mezghani and A. L. Swindlehurst, "Blind estimation of sparse broadband massive MIMO channels with ideal and one-bit ADCs," *IEEE Trans. Signal Process.*, vol. 66, no. 11, pp. 2972-2983, June 2018.
- [12] Hongting Zhang and Hsiao-Chun Wu, "Robust pilot detection techniques for channel estimation and symbol detection in OFDM systems," *IEEE Signal Process. Lett.*, vol. 22, no. 6, pp. 733-737, June 2015.
- [13] R. Shaked, N. Shlezinger and R. Dabora, "Joint estimation of carrier frequency offset and channel impulse response for linear periodic channels," *IEEE Trans. Commun.*, vol. 66, no. 1, pp. 302-319, Jan. 2018.
- [14] Y. Wang, G. Liu, F. Han and H. Qu, "Channel estimation and equalization for SS-OOFDM system with high mobility," *IEEE Wireless Commun. Lett.*, vol. 23, no. 1, pp. 92-95, Jan. 2019.
- [15] Chenhao Qi, Guosen Yue, Lenan Wu, and A. Nallanathan, "Pilot design for sparse channel estimation in OFDM-based cognitive radio systems," *IEEE Trans. on Veh. Technol.*, vol. 63, no. 2, pp. 982-987, Feb. 2014.
- [16] G. Liu, L. Zeng, H. Li, L. Xu, and Z. Wang, "Adaptive complex interpolator for channel estimation in pilot-aided OFDM system," *J. Commun. Networks*, vol. 15, no. 5, pp. 496-503, Oct. 2013.
- [17] Jung-Chieh Chen, Chao-Kai Wen, and Pangan Ting, "An efficient pilot design scheme for sparse channel estimation in OFDM systems," *IEEE Commun. Lett.*, vol. 17, no. 7, pp. 1352-1355, July 2013.
- [18] T. Lee, D. Sim, B. Seo and C. Lee, "Channel estimation scheme in oversampled frequency domain for FBMC-QAM systems based on prototype filter set," *IEEE Trans. Veh. Technol.*, vol. 68, no. 1, pp. 728-739, Jan. 2019.

- [19] P. Tan and N. Beaulieu, "Effect of channel estimation error on bit error probability in OFDM systems over Rayleigh and Ricean fading channels," *IEEE Trans. Commun.*, vol. 56, no. 4, pp. 675-685., Apr. 2008.
- [20] S. Tomasin and M. Butussi, "Analysis of interpolated channel estimation for mobile OFDM systems," *IEEE Trans. Commun.*, vol. 58, no. 5, pp. 1578-1588, May 2010.
- [21] M. Simko, P. Diniz, Qi Wang, and M. Rupp, "Adaptive pilot-symbol patterns for MIMO OFDM systems," *IEEE Trans. Wireless Commun.*, vol. 12, no. 9, pp. 4705-4715, Sep. 2013.
- [22] F. D'Agostini, S. Carboni, M. De Castro, F. De Castro, and D. Trindade, "Adaptive concurrent equalization applied to multicarrier OFDM systems," *IEEE Trans. Broadcast*, vol. 54, no. 3, pp. 441-447, Sep. 2008.
- [23] M. Henkel, C. Schilling and W. Schroer, "Comparison of channel estimation methods for pilot aided OFDM systems," in *Proc. IEEE VTC. Spring*, Dublin, 2007, pp. 1435-1439.
- [24] IEEE Standard for Information technology Telecommunications and information exchange between systems local and metropolitan area networks, specific requirements, Part 11: Wireless LAN Medium Access Control (MAC) and Physical Layer (PHY) Specifications, Amendment 4: Enhancements for Very High Throughput for Operation in Bands below 6 GHz, Dec. 2013.
- [25] M. Wu and P. Y. Kam, "Performance analysis and computational complexity comparison of sequence detection receivers with no explicit channel estimation," *IEEE Trans. on Veh. Technol.*, vol. 59, no. 5, pp. 2625-2631, Jun 2010.
- [26] W. C. Jakes, *Microwave Mobile Communications*. Piscataway, NJ: IEEE Press, 1994.
- [27] Seijas-Macias, Antonio, and Amilcar Oliveira. "An approach to distribution of the product of two normal variables," *Discussiones Mathematicae Probability and Statistics*, vol. 32, no. 1-2, pp. 87-99, 2012.
- [28] J. G. Proakis, and M. Salehi, *Digital communications*, 4th ed. New York: McGraw-Hill, 2001.
- [29] Borjesson, P., and C-E. Sundberg. "Simple approximations of the error function  $Q(x)$  for communications applications," *IEEE Trans. Commun.*, vol. 27, no. 3, pp. 639-643, March 1979.
- [30] M. Tariq, A. Al-Dweik, B. Mohammad, H. Saleh and T. Stouraitis, "Computational power analysis of wireless communications systems using operation-level power measurements," in *Proc. ICECTA*, Ras Al Khaimah, 2017, pp. 1-6.
- [31] D. Petrinovic, "Causal cubic splines: formulations, interpolation properties and implementations," *IEEE Trans. Signal Process.*, vol. 56, no. 11, pp. 5442-5453, Nov. 2008.
- [32] D. Lamb, L. F. O. Chamon and V. H. Nascimento, "Efficient filtering structure for spline interpolation and decimation," *IET Electron. Lett.*, vol. 52, no. 1, pp. 39-41, Aug. 1 2016.
- [33] ETSI TR 125 943 V9.0.0 (2010-02), Universal Mobile Telecommunications System (UMTS) Deployment Aspects, 3GPP TR 25.943, Release 9.